Y. J. Liu[1]
N. Nishimura
Y. Otani

Academic Center for Computing and Media Studies,
Kyoto University,
Kyoto 606-8501, Japan

T. Takahashi
Computational Astrophysics Labortory,
RIKEN,
Wako 351-0198, Japan

X. L. Chen
Department of Mechanical, Industrial and Nuclear Engineering,
University of Cincinnati,
Cincinnati, OH 45221-0072

H. Munakata
Academic Center for Computing and Media Studies,
Kyoto University,
Kyoto 6068501, Japan

A Fast Boundary Element Method for the Analysis of Fiber-Reinforced Composites Based on a Rigid-Inclusion Model

A new boundary element method (BEM) is developed for three-dimensional analysis of fiber-reinforced composites based on a rigid-inclusion model. Elasticity equations are solved in an elastic domain containing inclusions which can be assumed much stiffer than the host elastic medium. Therefore the inclusions can be treated as rigid ones with only six rigid-body displacements. It is shown that the boundary integral equation (BIE) in this case can be simplified and only the integral with the weakly-singular displacement kernel is present. The BEM accelerated with the fast multipole method is used to solve the established BIE. The developed BEM code is validated with the analytical solution for a rigid sphere in an infinite elastic domain and excellent agreement is achieved. Numerical examples of fiber-reinforced composites, with the number of fibers considered reaching above 5800 and total degrees of freedom above 10 millions, are solved successfully by the developed BEM. Effective Young's moduli of fiber-reinforced composites are evaluated for uniformly and "randomly" distributed fibers with two different aspect ratios and volume fractions. The developed fast multipole BEM is demonstrated to be very promising for large-scale analysis of fiber-reinforced composites, when the fibers can be assumed rigid relative to the matrix materials. [DOI: 10.1115/1.1825436]

1 Introduction

Modeling can play an important role in the analysis and design of fiber-reinforced composite materials. Mechanical properties and possible failure modes of these composites can be predicted early during the design stage using modeling techniques. However, modeling fiber-reinforced materials presents many challenges to numerical methods. Fibers in a composite can have different properties, shapes and sizes. They can be straight or curved, short or long, aligned or oriented arbitrarily, and distributed uniformly or randomly. All these factors make estimates of the mechanical properties of fiber-reinforced composites very difficult using the numerical methods. Often a representative volume element (RVE) containing only a few fibers may not be sufficient for accurately determining the effective properties of a composite. Large-scale models with hundreds or thousands of fibers may be deemed necessary in many situations. Unfortunately, modeling fibers, matrix, and possibly interphases between them as separate material domains in large-scale models is beyond the limit of current computing power. This has been the main reason that most of the current models of the fiber-reinforced composites based on the boundary integral equation and boundary element method (BIE/BEM) are two-dimensional ones with one or a few fibers considered in the RVEs (see, e.g., Refs. [1–8]). These models are adequate for the study of local properties, such as interfacial stresses and fractures, of a composite, but are often not sufficient for evaluating the overall mechanical properties of the composite. Therefore, models that can capture the overall behaviors of a composite without overwhelming computing resources are needed and will be beneficial in large-scale simulations. Using the rigid-inclusion model seems to be a feasible first step in large-scale simulations for investigating the interactions of fibers, load transfer mechanism and effective properties of a composite. The rigid-inclusion approximation is valid when the fibers have much higher values of stiffness compared with that of the matrix. This approximation can significantly reduce the modeling complexity for the analysis, as will be demonstrated in this paper.

There are two approaches regarding whether or not to further simplify the geometries for modeling rigid inclusions. One approach treats the rigid inclusions as they are without further simplifying their geometries, which consequently requires 3D models for rigid inclusions. The other approach treats slender rigid inclusions, as in the case of long-fiber-reinforced composites, as rigid-line inclusions, where the geometry of an inclusion is reduced to a *line*. This rigid-line inclusion model is valid when the aspect ratio of an inclusion is large. It is also efficient in modeling of rigid-line inclusions because of the simplified geometry. Only 2D models of rigid-line inclusions in a medium have been studied so far.

In the analysis of rigid-line inclusions, also called anticracks in a 2D elastic domain [9], many research results have been reported in the literature. Boundary integral equation and boundary element method have been found especially suitable for the analysis of rigid-line inclusions, since cracks in 2D, the counter part of rigid lines, have been studied intensively by using the BIEs. Many of the results for crack analysis can be extended readily to the analysis of rigid-line inclusions. In the early 1990s, the group of Hu, Chandra and Huang made considerable contributions to the study of rigid-line inclusions in a matrix using the boundary inte-

[1]Corresponding author. On leave from the Department of Mechanical, Industrial and Nuclear Engineering, University of Cincinnati, P.O. Box 210072, Cincinnati, OH 45221-0072. e-mail: yijun.liu@uc.edu

Contributed by the Applied Mechanics Division of THE AMERICAN SOCIETY OF MECHANICAL ENGINEERS for publication in the ASME JOURNAL OF APPLIED MECHANICS. Manuscript received by the Applied Mechanics Division, January 29, 2004; final revision; May 22, 2004. Associate Editor: M. Mukherjee. Discussion on the paper should be addressed to the Editor, Professor Robert M. McMeeking, Journal of Applied Mechanics, Department of Mechanical and Environmental Engineering, University of California-Santa Barbara, Santa Barbara, CA 93106-5070, and will be accepted until four months after final publication of the paper itself in the ASME JOURNAL OF APPLIED MECHANICS.

gral equation method for 2D cases. Some of their analytical and numerical results can be found in Refs. [10–14]. In these works, the rigid lines embedded in an infinite space are represented by distributions of tractions along the rigid lines (as compared to distributions of dislocations for cracks) and integral equations are established using the Green's functions. The interactions of rigid lines with cracks and the effects of rigid lines on the effective elastic material properties of composites were successfully studied using this approach for 2D models [10–14]. Extensive review of the earlier theoretical work on the elasticity study of rigid-line inclusions in a solid can also be found in Refs. [10–14]. Recently, there seems to be a renewed interest in the study of rigid-line inclusions using the BIEs. In Ref. [15], Leite, Coda, and Venturini reported a 2D BEM coupled with the finite elements that are used to model the bar inclusions in a matrix. These bar inclusions, representing fibers in a matrix, are assumed to be rigid within any cross section of a bar, but can deform along the axial direction in their models. The displacement and stress fields near the line inclusions are studied by this approach. In a recent work [16], Dong, Lo, and Cheung developed a hypersingular BIE approach for the analysis of interactions of rigid-line inclusions with cracks in a 2D elastic medium. Stress intensity factors at the tips of rigid lines are computed with this hypersingular BIE approach and compared with analytical solutions. In all the results mentioned above, only 2D models with a small number (less than 10) of rigid-line inclusions have been considered. Most recently, Nishimura and Liu [17] used the fast multipole BEM to solve rigid-line inclusion models in the context of 2D thermal analysis. The rigid-line concept in the thermal case means line inclusions with much higher thermal conductivities than that of the matrix material. A hypersingular BIE was employed and up to 10 000 line inclusions were studied. The effective thermal conductivity of a 2D medium (thin films) containing rigid lines were successfully evaluated using the 2D RVEs embedded in an infinite plane in Ref. [17].

In the case of modeling rigid inclusions as 2D or 3D objects without simplifying their geometries, Ingber and Papathanasiou's work [18] seems to be the only reported one using the boundary element method. The full conventional BIE for Navier's equation governing an *incompressible* medium containing rigid fibers is solved in [18] in order to determine the effective moduli of composites with different fiber volume fractions and aspect ratios. Constant boundary elements were employed to discretize the BIE which contains the singular as well as weakly-singular kernels. Parallel computing was used to solve the BEM equations. Up to 200 short, aligned rigid fibers, with the total degrees of freedom (DOFs) of about 12 000, were successfully solved by the developed BEM approach. Very good agreement of the evaluated effective moduli using their BEM approach and analytical results is reported in [18], which clearly demonstrates that the rigid-fiber model is very promising and the BEM is very efficient for analyzing fiber-reinforced composites. In the field of fluid mechanics, there are many research results concerning the flows of fluids around rigid solids. Two recent references using the boundary element method for modeling rigid bodies in fluids can be found in Refs. [19], [20]. In particular, in Ref. [19], an indirect BIE of the first kind using the single-layer potential is developed for solving Stokes equations and this approach is found to be very stable and more amenable to fast iterative solvers.

The boundary element method based on the BIEs is a natural way to model inclusion problems, due to its reduction of the dimension of the problem domain and high accuracy. With the development of the fast multipole methods (FMM) (see a recent review in Ref. [21]) for solving boundary integral equations, large models with several million degrees of freedom can be solved readily on a desktop computer. Rokhlin, Greengard, and coworkers, who pioneered the FMM, have done extensive research on the FMM for inclusion problems in the context of potential fields as well as elastic fields in two-dimensional domains (see, Ref. [22] and related papers in Refs. [23–25]). Rodin and coworkers [26] have formulated the BIE for 3D elastic inclusion problems using the FMM. Solutions for up to 343 spherical voids in an elastic domain were computed using their parallel FMM BEM code (with total DOFs about 400 000) [26]. Some other development of the fast multipole BEM can be found in Refs. [27], [28] for general elasticity problems, and in [29–31] for crack problems. With the advances of new composites, new modeling approaches that can handle even larger numbers of fibers in an RVE need to be developed. The rigid-inclusion approach seems to be a feasible first approximation with the current computing capabilities. All these demands in materials research and progresses in the BEM suggest that the rigid-inclusion models and the fast multipole BEM may play a significant role in the analysis of fiber-reinforced composites.

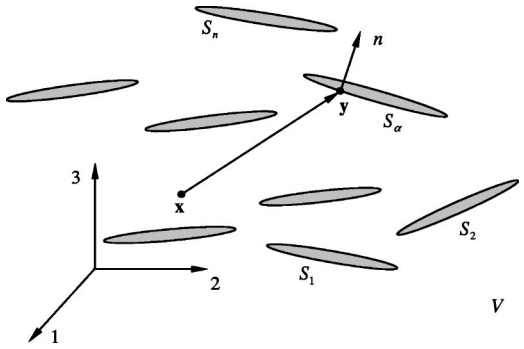

Fig. 1 A 3D infinite elastic medium (R^3) embedded with rigid inclusions

In this paper, a new BIE formulation is presented for the analysis of rigid inclusions in a general 3D isotropic elastic medium based on the general direct BIE formulation. The BIE contains only the displacement kernel and the influence of the traction kernel is implied in the coefficient of the free displacement term. Although this integral equation is essentially (not exactly) a Fredholm integral equation of the first kind, it is suitable for numerical solutions with iterative solvers because a good preconditioner is available. The BEM accelerated by the fast multipole method is used to solve the established BIE and the preconditioned system of equations is found to be well conditioned. The analytical solution of a rigid sphere in an infinite elastic domain is used to validate the developed BEM code and excellent agreement is achieved. Examples for modeling fiber-reinforced composites, with the number of fibers reaching above 5800 and total DOFs above 10 millions, are successfully solved by the developed fast multipole BEM. Effective Young's moduli of fiber-reinforced composites are evaluated for uniformly and ''randomly'' distributed and oriented fibers with two different aspect ratios and volume fractions. The developed fast multipole BEM is demonstrated to be very promising for large-scale analysis of fiber-reinforced composites, when the fibers can be assumed rigid relative to the matrix. It can also be applied to modeling other inclusion problems.

2 BIE Formulation for an Elastic Medium Containing Rigid Inclusions

The boundary integral equation for the analysis of an elastic domain containing rigid inclusions is derived in this section. This new and simplified BIE formulation contains only one integral with the displacement kernel and thus can facilitate more efficient computation. Consider a 3D infinite elastic domain V embedded with n rigid inclusions (Fig. 1). The matrix is loaded with a remote stress or displacement field. The displacement at a point inside the domain is given by the following direct representation integral (see, e.g., [32]):

$$\mathbf{u}(\mathbf{x}) = \int_S [\mathbf{U}(\mathbf{x},\mathbf{y})\mathbf{t}(\mathbf{y}) - \mathbf{T}(\mathbf{x},\mathbf{y})\mathbf{u}(\mathbf{y})]dS(\mathbf{y}) + \mathbf{u}^{\infty}(\mathbf{x}), \quad \forall \mathbf{x} \in V, \tag{1}$$

where $\mathbf{u}$ and $\mathbf{t}$ are the displacement and traction vectors, respectively; $S = \cup_\alpha S_\alpha$ with S_α being the boundary of the αth rigid inclusion (Fig. 1); and $\mathbf{u}^\infty$ the undisturbed displacement field when a remote stress or displacement field is applied and the rigid inclusions are not present (This term is similar to that for an incident wave in the elastodynamic case [33]). For a finite domain model, this term will not be present in Eq. (1). The two kernel functions $\mathbf{U}(\mathbf{x},\mathbf{y})$ and $\mathbf{T}(\mathbf{x},\mathbf{y})$ in Eq. (1) are the displacement and traction components in the fundamental solution (Kelvin's solution), respectively, which can be found in any BEM references (see, e.g., [34–37]).

Before we let the source point $\mathbf{x}$ approach the boundary S to derive the boundary integral equation, we first consider the rigid-body motions of each inclusion. For a rigid inclusion enclosed by S_α, the displacement at any point $\mathbf{y}$ can be described by the rigid-body motions as:

$$\mathbf{u}(\mathbf{y}) = \mathbf{d} + \boldsymbol{\omega} \times \mathbf{p}(\mathbf{y}), \tag{2}$$

where $\mathbf{d}$ is the rigid-body translational displacement vector, $\boldsymbol{\omega}$ the rotation vector, and $\mathbf{p}$ a position vector for point $\mathbf{y}$ measured from a reference point (such as the center of the inclusion). Consider a *complement* problem in the interior region enclosed by S_α and filled with the same material as that of domain V. Then the following representation integral holds:

$$\mathbf{0} = \int_{S_\alpha} [\tilde{\mathbf{U}}(\mathbf{x},\mathbf{y})\tilde{\mathbf{t}}(\mathbf{y}) - \tilde{\mathbf{T}}(\mathbf{x},\mathbf{y})\tilde{\mathbf{u}}(\mathbf{y})]dS(\mathbf{y}), \quad \forall \mathbf{x} \in V, \tag{3}$$

where $\tilde{\mathbf{u}}$ and $\tilde{\mathbf{t}}$ are the displacement and traction vectors, respectively, for this complement problem; $\tilde{\mathbf{U}} = \mathbf{U}$ and $\tilde{\mathbf{T}} = -\mathbf{T}$ as in Eq. (1) (the normal for the region enclosed by S_α is in the opposite direction of n shown in Fig. 1). Any rigid-body motion is a solution to the elasticity equations for the complement problem. Thus, the following solution:

$$\tilde{\mathbf{u}}(\mathbf{y}) = \mathbf{u}(\mathbf{y}) = \mathbf{d} + \boldsymbol{\omega} \times \mathbf{p}(\mathbf{y}), \quad \tilde{\mathbf{t}}(\mathbf{y}) = \mathbf{0}$$

satisfies the representation integral (3). Substituting these results into (3), we obtain:

$$\int_{S_\alpha} \mathbf{T}(\mathbf{x},\mathbf{y})[\mathbf{d} + \boldsymbol{\omega} \times \mathbf{p}(\mathbf{y})]dS(\mathbf{y}) = \mathbf{0}, \quad \forall \mathbf{x} \in V,$$

or

$$\int_{S_\alpha} \mathbf{T}(\mathbf{x},\mathbf{y})\mathbf{u}(\mathbf{y})dS(\mathbf{y}) = \mathbf{0}, \quad \forall \mathbf{x} \in V, \tag{4}$$

for the region enclosed by S_α ($\alpha = 1,2,\ldots,n$). This is exactly the second integral with the $\mathbf{T}$ kernel in Eq. (1) on one inclusion. Therefore, the integral in Eq. (1) involving the $\mathbf{T}$ kernel vanishes and Eq. (1) reduces to:

$$\mathbf{u}(\mathbf{x}) = \int_S \mathbf{U}(\mathbf{x},\mathbf{y})\mathbf{t}(\mathbf{y})dS(\mathbf{y}) + \mathbf{u}^{\infty}(\mathbf{x}), \quad \forall \mathbf{x} \in V, \tag{5}$$

for all *rigid* inclusions ($S = \cup_\alpha S_\alpha$). This representation integral can be applied to evaluate the displacement field at any point inside the domain V, once the tractions on the surfaces of the rigid inclusions are obtained. The stress field at any point in the domain can also be evaluated by taking derivatives of expression (5) and applying the Hook's law.

To obtain the traction values on surfaces of the rigid inclusions, we let the source point $\mathbf{x}$ approach the boundary S to arrive at the following boundary integral equation:

$$\mathbf{u}(\mathbf{x}) = \int_S \mathbf{U}(\mathbf{x},\mathbf{y})\mathbf{t}(\mathbf{y})dS(\mathbf{y}) + \mathbf{u}^{\infty}(\mathbf{x}), \quad \forall \mathbf{x} \in S = \underset{\alpha}{\cup} S_\alpha, \tag{6}$$

in which no jump term arises since the $\mathbf{U}$ kernel is only weakly singular [34–37]. This BIE for rigid-inclusion problems is extremely compact and simple, in which only the weakly-singular kernel needs to be handled. Analytical solutions for rigid-inclusion problems may be obtained for simple geometries by using this BIE formulation.

Although the BIE (6) for rigid inclusions are much simpler to handle than the BIE for elastic inclusions, it requires additional considerations, that is, the rigid-body motions of each inclusion, expressed by Eq. (2) that contains six unknowns ($\mathbf{d}$ and $\boldsymbol{\omega}$ vectors) for each inclusion. Additional equations are needed to supplement BIE (6). These equations can be obtained by considering the equilibrium of each inclusion, that is, the following (six scalar) equations:

$$\int_{S_\alpha} \mathbf{t}(\mathbf{y})dS(\mathbf{y}) = \mathbf{0}; \tag{7}$$

$$\int_{S_\alpha} \mathbf{p}(\mathbf{y}) \times \mathbf{t}(\mathbf{y})dS(\mathbf{y}) = \mathbf{0}; \tag{8}$$

for $\alpha = 1,2,\ldots,n$. Expression (7) represents the equilibrium of the forces, while expression (8) that of the moments, for the rigid inclusions. BIE (6) and Eqs. (2), (7), and (8) are simultaneously solved to obtain the unknown rigid-body motions $\mathbf{d}$ and $\boldsymbol{\omega}$, and traction $\mathbf{t}$ for all the inclusions.

It should be pointed out that BIE in (6) is essentially a Fredholm integral equation of the first kind, although not exactly since it contains additional finite number of unknowns $\mathbf{d}$ and $\boldsymbol{\omega}$ for each inclusion. Integral equations of the first kind are usually considered not suitable for numerical solutions with iterative solvers. This problem can be resolved in two ways. Namely, we either convert the BIE into an equivalent equation of the second kind, or use a preconditioner after the discretization. One may possibly replace BIE (6) by a second kind integral equation of the following form as one uses instead the traction equation corresponding to (6):

$$\tfrac{1}{2}\mathbf{t}(\mathbf{x}) = \int_S T\mathbf{U}(\mathbf{x},\mathbf{y})\mathbf{t}(\mathbf{y})dS(\mathbf{y}) + T\mathbf{u}^{\infty}(\mathbf{x}), \quad \forall \mathbf{x} \in S = \underset{\alpha}{\cup} S_\alpha,$$

where T is the traction operator which is applied to $\mathbf{x}$. Unfortunately, the solution to this equation is not unique. We therefore decided to use BIE (6) for the analysis since we can find a good preconditioner for the system obtained after discretization of (6), as we shall see later.

In 2D, BIE (6) will degenerate in the limit as the aspect ratio of an inclusion tends to infinity, that is, equations generated by using BIE (6) on the two opposing boundaries of a slender inclusion will be identical and thus not enough equations will be available for solving the BIE for separate tractions. In this case, the sum of tractions across the inclusion can be used as a new variable in BIE (6) to derive a new equation. Different Green's function formulations can also be employed to consider rigid lines based on the work in Refs. [9–15], which may turn out to be equivalent with the equation based on BIE (6). Like the crack cases, hypersingular BIE formulations can also be applied, as has been done recently in [16] for 2D elasticity, and in [17] for 2D thermal analysis of line inclusions. New BIE formulations for rigid-line inclusion problems in 3D, however, still remain to be developed.

3 The Fast Multipole Method

The fast multipole method [21–31] is employed to accelerate the BEM solution of the BIE for rigid inclusions. In recent years, the fast multipole method has been demonstrated to be especially good for solving problems with large numbers of cracks and inclusions in both 2D and 3D cases. Using the fast multipole method for the BEM, the solution time of a problem is reduced to order $O(N)$, instead of $O(N^2)$ as in the traditional BEM (with N here being the number of equations). The memory requirement is

also reduced since the iterative solver (such as GMRES) does not require the storage of the entire matrix in the memory. Thus, large models that had to be solved on a supercomputer in the past can now be solved on a desktop computer.

In the following, we briefly list the main results of the fast multipole method for the developed BIE (6) to show the essence of this powerful approach to solving BIEs. Complete formulations and steps in implementations of the FMM for elastostatic problems can be found in Refs. [38,39]. Other formulations using different FMM approaches for general elasticity problems can be found in Refs. [26–28].

We start with the following form of the fundamental solution (index notation is employed here, where repeated indices imply summations):

$$U_{ij}(\mathbf{x},\mathbf{y})=\frac{1}{8\pi\mu}\left(\delta_{ij}\frac{2}{r}-\frac{\lambda+\mu}{\lambda+2\mu}\frac{\partial}{\partial x_i}\frac{x_j-y_j}{r}\right), \tag{9}$$

where λ and μ are the Lamé constants, δ_{ij} the Kronecker symbol, and $r=r(\mathbf{x},\mathbf{y})$ the distance between the source point $\mathbf{x}$ and field point $\mathbf{y}$. The following identity holds:

$$\frac{1}{r(\mathbf{x},\mathbf{y})}=\sum_{n=0}^{\infty}\sum_{m=-n}^{n}S_{n,m}(\overrightarrow{\mathbf{Ox}})\overline{R_{n,m}}(\overrightarrow{\mathbf{Oy}}), \tag{10}$$

for $|\overrightarrow{\mathbf{Oy}}|<|\overrightarrow{\mathbf{Ox}}|$, in which $\mathbf{O}$ represents a third point, $R_{n,m}$ and $S_{n,m}$ are solid harmonic functions defined in Refs. [38,39], and $\overline{(\ )}$ means the complex conjugate. Substituting (10) into (9), we arrive at:

$$U_{ij}(\mathbf{x},\mathbf{y})=\frac{1}{8\pi\mu}\sum_{n=0}^{\infty}\sum_{m=-n}^{n}[F_{ij,n,m}(\overrightarrow{\mathbf{Ox}})\overline{R_{n,m}}(\overrightarrow{\mathbf{Oy}})+G_{i,n,m}(\overrightarrow{\mathbf{Ox}})(\overrightarrow{\mathbf{Oy}})_j\overline{R_{n,m}}(\overrightarrow{\mathbf{Oy}})], \tag{11}$$

where,

$$F_{ij,n,m}(\overrightarrow{\mathbf{Ox}})=\frac{\lambda+3\mu}{\lambda+2\mu}\delta_{ij}S_{n,m}(\overrightarrow{\mathbf{Ox}})-\frac{\lambda+\mu}{\lambda+2\mu}(\overrightarrow{\mathbf{Ox}})_j\frac{\partial}{\partial x_i}S_{n,m}(\overrightarrow{\mathbf{Ox}}),$$

$$G_{i,n,m}(\overrightarrow{\mathbf{Ox}})=\frac{\lambda+\mu}{\lambda+2\mu}\frac{\partial}{\partial x_i}S_{n,m}(\overrightarrow{\mathbf{Ox}}).$$

The significance of expression (11) is that the kernel $U_{ij}(\mathbf{x},\mathbf{y})$ is now a sum of functions in the form of $k_n^{(1)}(\mathbf{x}-\mathbf{O})k_n^{(2)}(\mathbf{y}-\mathbf{O})$, which will facilitate integrations independent of the source point $\mathbf{x}$ and thus reduce the number of integrals to compute. To see this, consider the integral in BIE (6) on a subdomain S_o of S away from the source point $\mathbf{x}$. Applying expression (11), with point $\mathbf{O}$ being close to subdomain S_o, we obtain:

$$\int_{S_o}U_{ij}(\mathbf{x},\mathbf{y})t_j(\mathbf{y})dS(\mathbf{y})=\frac{1}{8\pi\mu}\sum_{n=0}^{\infty}\sum_{m=-n}^{n}[F_{ij,n,m}(\overrightarrow{\mathbf{Ox}})\overline{M_{j,n,m}}(\mathbf{O})+G_{i,n,m}(\overrightarrow{\mathbf{Ox}})\overline{M_{n,m}}(\mathbf{O})], \tag{12}$$

in which,

$$M_{j,n,m}(\mathbf{O})=\int_{S_o}R_{n,m}(\overrightarrow{\mathbf{Oy}})t_j(\mathbf{y})dS(\mathbf{y}), \tag{13}$$

$$M_{n,m}(\mathbf{O})=\int_{S_o}(\overrightarrow{\mathbf{Oy}})_jR_{n,m}(\overrightarrow{\mathbf{Oy}})t_j(\mathbf{y})dS(\mathbf{y}), \tag{14}$$

are called the *multipole moments* for given n and m. Note that these four moments are independent of the location of the source point $\mathbf{x}$ and thus only need to be calculated once for all locations of the source point away from S_o (S_o will be a cell in FMM and $\mathbf{O}$ will be the center of this cell). To evaluate the integral using Eq. (12), only a small number of terms are required in the expansion. For example, using ten terms for n in these expansions has been found sufficient for most problems. Further details of the FMM in the context of general 3D elastostatic problems and used in this work can be found in Refs. [38,39].

The fast multipole BEM code developed for the current analysis of rigid inclusions in 3D elastic media is based on the FMM BEM code that was developed at the Kyoto University for general elasticity problems [38]. This earlier FMM code has been tested on some large-scale stress analysis problems of regular structures. More details on the FMM for the BEM and its implementations in solving other types of problems can be found in Refs. [21], [39].

4 Discretization of the BIE

The boundary element method, accelerated by the fast multipole method, is applied to solve BIE (6) together with Eqs. (2), (7), and (8). In this paper, constant triangular boundary elements are used to discretize these equations over the surfaces of the inclusions. One node is placed on each surface element and the field variable (traction) is assumed to be constant over each element which is a flat triangular area defined by its three corner points. Although constant elements may not be as accurate as linear or quadratic surface elements, they have certain advantages over other higher-order elements. For example, all the integrals involved in using the constant elements can be evaluated analytically in both 2D and 3D cases. (As a matter of fact, it is not impossible to carry out analytical integrations for any planar elements with arbitrary polynomial basis functions. But the results will be quite complicated.) This avoids the use of any numerical integration in the BEM and hence guarantees the accuracy in the evaluation of all integrals when the source point $\mathbf{x}$ is very close to an element of integration (which happens when many inclusions are closely packed in a model).

If the nodes are grouped together for each inclusion, numbered on one inclusion after another, then a discretized form of the BIE (6) can be written as:

$$\begin{Bmatrix}\tilde{\mathbf{u}}_1\\ \tilde{\mathbf{u}}_2\\ \vdots\\ \tilde{\mathbf{u}}_n\end{Bmatrix}=\begin{bmatrix}\tilde{\mathbf{U}}_{11} & \tilde{\mathbf{U}}_{12} & \cdots & \tilde{\mathbf{U}}_{1n}\\ \tilde{\mathbf{U}}_{21} & \tilde{\mathbf{U}}_{22} & \cdots & \tilde{\mathbf{U}}_{2n}\\ \vdots & \vdots & \ddots & \vdots\\ \tilde{\mathbf{U}}_{n1} & \tilde{\mathbf{U}}_{n2} & \cdots & \tilde{\mathbf{U}}_{nn}\end{bmatrix}\begin{Bmatrix}\tilde{\mathbf{t}}_1\\ \tilde{\mathbf{t}}_2\\ \vdots\\ \tilde{\mathbf{t}}_n\end{Bmatrix}+\begin{Bmatrix}\tilde{\mathbf{u}}_1^{\infty}\\ \tilde{\mathbf{u}}_2^{\infty}\\ \vdots\\ \tilde{\mathbf{u}}_n^{\infty}\end{Bmatrix}, \tag{15}$$

where n is the total number of inclusions being considered; $\tilde{\mathbf{u}}_\alpha$ and $\tilde{\mathbf{t}}_\alpha$ the nodal displacement and traction vector for inclusion α, respectively; $\tilde{\mathbf{u}}_\alpha^{\infty}$ the given remote displacement vector evaluated on inclusion α; and $\tilde{\mathbf{U}}_{\alpha\beta}$ the coefficient matrix obtained from the (analytical) integration of the displacement kernel over inclusion β when the source point $\mathbf{x}$ is located on inclusion α. From Eq. (2), the nodal displacement vector on an inclusion α can be related to the rigid-body translation $\mathbf{d}$ and rotation $\boldsymbol{\omega}$ of that inclusion by the following expression:

$$\tilde{\mathbf{u}}_\alpha=\begin{Bmatrix}\mathbf{u}_1\\ \mathbf{u}_2\\ \vdots\\ \mathbf{u}_m\end{Bmatrix}=\begin{bmatrix}\mathbf{a}_1\\ \mathbf{a}_2\\ \vdots\\ \mathbf{a}_m\end{bmatrix}\boldsymbol{\varphi}_\alpha=\mathbf{A}_\alpha\boldsymbol{\varphi}_\alpha, \tag{16}$$

in which $\mathbf{u}_i$ is the nodal displacement vector at node i (with m being the number of nodes on inclusion α); $\mathbf{a}_i$ the transformation matrix for each node i on inclusion α given by [see Eq. (2)]:

$$\mathbf{a}_i=\begin{bmatrix}1 & 0 & 0 & 0 & p_3 & -p_2\\ 0 & 1 & 0 & -p_3 & 0 & p_1\\ 0 & 0 & 1 & p_2 & -p_1 & 0\end{bmatrix}, \tag{17}$$

with p_k being the component of the position vector $\mathbf{p}$ for node i; and finally in (16), $\boldsymbol{\varphi}_\alpha$ is the rigid-body displacement vector for inclusion α, defined by:

$$\boldsymbol{\varphi}_\alpha=[d_1\ \ d_2\ \ d_3\ \ \omega_1\ \ \omega_2\ \ \omega_3]^T, \tag{18}$$

for $\alpha=1,2,\ldots,n$. The system of equations (15) is supplemented with the following ones from discretizations of Eqs. (7) and (8) on each inclusion α:

$$\mathbf{B}_\alpha \tilde{\mathbf{t}}_\alpha = \mathbf{0}, \tag{19}$$

for $\alpha=1,2,\ldots,n$, in which $\mathbf{B}_\alpha$ is a $6\times 3m$ coefficient matrix obtained by evaluating Eqs. (7) and (8) on inclusion α.

With results in (16)–(18), the discretized BIE (15) and Eq. (19) can now be combined to provide the following form of the system of equations:

$$\begin{bmatrix} -\tilde{\mathbf{U}}_{11} & -\tilde{\mathbf{U}}_{12} & \cdots & -\tilde{\mathbf{U}}_{1n} & \mathbf{A}_1 & \mathbf{0} & \cdots & \mathbf{0} \\ -\tilde{\mathbf{U}}_{21} & -\tilde{\mathbf{U}}_{22} & \cdots & -\tilde{\mathbf{U}}_{2n} & \mathbf{0} & \mathbf{A}_2 & \cdots & \mathbf{0} \\ \vdots & \vdots & \ddots & \vdots & \vdots & \vdots & \ddots & \vdots \\ -\tilde{\mathbf{U}}_{n1} & -\tilde{\mathbf{U}}_{n2} & \cdots & -\tilde{\mathbf{U}}_{nn} & \mathbf{0} & \mathbf{0} & \cdots & \mathbf{A}_n \\ \mathbf{B}_1 & \mathbf{0} & \cdots & \mathbf{0} & \mathbf{0} & \mathbf{0} & \cdots & \mathbf{0} \\ \mathbf{0} & \mathbf{B}_2 & \cdots & \mathbf{0} & \mathbf{0} & \mathbf{0} & \cdots & \mathbf{0} \\ \vdots & \vdots & \ddots & \vdots & \vdots & \vdots & \ddots & \vdots \\ \mathbf{0} & \mathbf{0} & \cdots & \mathbf{B}_n & \mathbf{0} & \mathbf{0} & \cdots & \mathbf{0} \end{bmatrix} \begin{Bmatrix} \tilde{\mathbf{t}}_1 \\ \tilde{\mathbf{t}}_2 \\ \vdots \\ \tilde{\mathbf{t}}_n \\ \boldsymbol{\varphi}_1 \\ \boldsymbol{\varphi}_2 \\ \vdots \\ \boldsymbol{\varphi}_n \end{Bmatrix} = \begin{Bmatrix} \tilde{\mathbf{u}}_1^\infty \\ \tilde{\mathbf{u}}_2^\infty \\ \vdots \\ \tilde{\mathbf{u}}_n^\infty \\ \mathbf{0} \\ \mathbf{0} \\ \vdots \\ \mathbf{0} \end{Bmatrix}. \tag{20}$$

There are $3N+6n$ equations in the above system (with $N=m\times n$, being the total number of nodes on all inclusions), which are sufficient for solving the $6n$ unknown rigid-body displacements and rotations ($\boldsymbol{\varphi}_\alpha$) of the n inclusions, and the $3N$ unknown traction components ($\tilde{\mathbf{t}}_\alpha$) at the N boundary nodes over all the inclusions. Note that in the above system, the dimension for submatrix $\mathbf{A}_\alpha$ is $3m\times 6$ and for $\mathbf{B}_\alpha$ is $6\times 3m$. Both are not square matrices (the number of nodes per inclusion m can be large). If all the inclusions are of the same size and shape, and meshed in the same way, then both the submatrices $\mathbf{A}_\alpha$ and $\mathbf{B}_\alpha$ can be computed only once for all the inclusions.

The iterative solver GMRES is used to solve the system of equations in Eq. (20), in which the multiplication of the (coefficient) matrix and (approximate solution) vector in each iteration are obtained by using the fast multipole method. In the FMM, the maximum depth of the oct-tree structure is below 10 levels. Direct integrations for near field interactions are computed during each iteration and are not stored to save the memory space. As for the preconditioner, we use the following (''diagonal'') matrix:

$$\mathbf{M}=\begin{bmatrix} -\tilde{\mathbf{U}}_{11} & \mathbf{0} & \cdots & \mathbf{0} & \mathbf{A}_1 & \mathbf{0} & \cdots & \mathbf{0} \\ \mathbf{0} & -\tilde{\mathbf{U}}_{22} & \cdots & \mathbf{0} & \mathbf{0} & \mathbf{A}_2 & \cdots & \mathbf{0} \\ \vdots & \vdots & \ddots & \vdots & \vdots & \vdots & \ddots & \vdots \\ \mathbf{0} & \mathbf{0} & \cdots & -\tilde{\mathbf{U}}_{nn} & \mathbf{0} & \mathbf{0} & \cdots & \mathbf{A}_n \\ \mathbf{B}_1 & \mathbf{0} & \cdots & \mathbf{0} & \mathbf{0} & \mathbf{0} & \cdots & \mathbf{0} \\ \mathbf{0} & \mathbf{B}_2 & \cdots & \mathbf{0} & \mathbf{0} & \mathbf{0} & \cdots & \mathbf{0} \\ \vdots & \vdots & \ddots & \vdots & \vdots & \vdots & \ddots & \vdots \\ \mathbf{0} & \mathbf{0} & \cdots & \mathbf{B}_n & \mathbf{0} & \mathbf{0} & \cdots & \mathbf{0} \end{bmatrix}. \tag{21}$$

The system in (20) is right-preconditioned with this matrix. The inverse of $\mathbf{M}$ is easily obtained as:

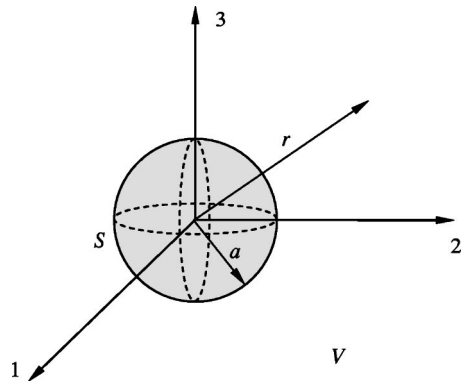

Fig. 2 A rigid sphere in an infinite elastic domain *V*

$$\mathbf{M}^{-1}=\begin{bmatrix} \mathbf{P}_1 & \mathbf{0} & \cdots & \mathbf{0} & \mathbf{Q}_1 & \mathbf{0} & \cdots & \mathbf{0} \\ \mathbf{0} & \mathbf{P}_2 & \cdots & \mathbf{0} & \mathbf{0} & \mathbf{Q}_2 & \cdots & \mathbf{0} \\ \vdots & \vdots & \ddots & \vdots & \vdots & \vdots & \ddots & \vdots \\ \mathbf{0} & \mathbf{0} & \cdots & \mathbf{P}_n & \mathbf{0} & \mathbf{0} & \cdots & \mathbf{Q}_n \\ \mathbf{R}_1 & \mathbf{0} & \cdots & \mathbf{0} & \mathbf{S}_1 & \mathbf{0} & \cdots & \mathbf{0} \\ \mathbf{0} & \mathbf{R}_2 & \cdots & \mathbf{0} & \mathbf{0} & \mathbf{S}_2 & \cdots & \mathbf{0} \\ \vdots & \vdots & \ddots & \vdots & \vdots & \vdots & \ddots & \vdots \\ \mathbf{0} & \mathbf{0} & \cdots & \mathbf{R}_n & \mathbf{0} & \mathbf{0} & \cdots & \mathbf{S}_n \end{bmatrix},$$

where

$$\begin{bmatrix} \mathbf{P}_i & \mathbf{Q}_i \\ \mathbf{R}_i & \mathbf{S}_i \end{bmatrix} = \begin{bmatrix} -\tilde{\mathbf{U}}_{ii} & \mathbf{A}_i \\ \mathbf{B}_i & \mathbf{0} \end{bmatrix}^{-1}, \quad \text{for inclusion } i=1,2,\ldots,n. \tag{22}$$

Physically speaking, inverting the matrix on the right-hand side of (22) means to solve a rigid-inclusion problem for the whole space just containing one inclusion (ith one). The inversion in (22) is a small operation which can be carried out efficiently with any direct solver for a matrix equation. With this preconditioning, the upper-right and lower-left submatrices in (20) reduce to zero matrices, while the lower-right submatrix and the block diagonals in the upper-left submatrix are converted into identity matrices. This is essentially equivalent to converting the original integral equation in (6) into another equation of the second kind whose solution is unique. The system thus obtained is well conditioned and the solutions are stable, as shown in the following numerical examples.

5 Numerical Examples

The developed fast BEM for the analysis of rigid inclusions is first validated using a test case of a single rigid sphere for which the analytical solution can be found readily. Then, the BEM code is applied to study the fiber-reinforced composites using the rigid-inclusion model.

5.1 A Rigid Sphere in an Infinite Elastic Medium. To validate the developed new BIE formulation and its BEM implementation for the study of rigid-inclusion models of fiber-reinforced composites, a rigid sphere in an infinite elastic medium is considered first (Fig. 2). The elastic medium containing the rigid sphere is loaded with a far-field triaxial stress σ^∞. The analytical solution for this axisymmetric problem can be obtained readily using basic elasticity theory [40] or the equivalent inclusion method [41]. The radial displacement, radial and tangential stresses in the elastic domain are found to be:

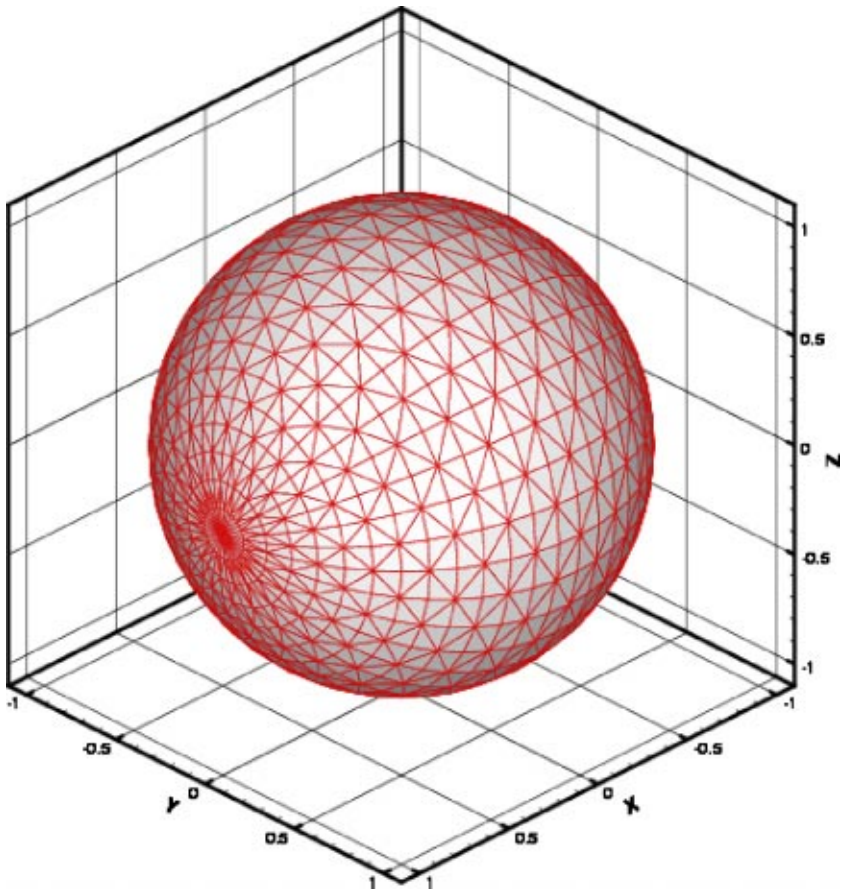

Fig. 3 A boundary element model of the sphere (with 1944 surface elements)

$$u_r(r) = \frac{(1-2\nu)\sigma^\infty}{E}\left(1-\frac{a^3}{r^3}\right)r, \tag{23}$$

$$\sigma_r(r) = \sigma^\infty\left[1+\frac{2(1-2\nu)}{1+\nu}\frac{a^3}{r^3}\right], \tag{24}$$

$$\sigma_\theta(r) = \sigma^\infty\left[1-\frac{1-2\nu}{1+\nu}\frac{a^3}{r^3}\right], \tag{25}$$

respectively, where a is the radius of the sphere, E the Young's modulus, and ν the Poisson's ratio of the elastic medium. Note that $u_r(a)=0$, which is the result for a rigid sphere.

The convergence of the BEM is studied with several boundary element meshes for the sphere. The finest mesh used (with 1944 elements) is shown in Fig. 3. The radial stress computed by the BEM on the surface is compared with the analytical solution [Eq. (24)] and the relative errors are plotted in Fig. 4 for different meshes with increasing numbers of elements. The error with the coarsest mesh (120 elements) is 4.93%, while that with the finest mesh (1944 elements) is 0.19%. The convergence of the BEM results is achieved. The field displacement and stresses within the elastic domain are plotted in Figs. 5 and 6, respectively, for the coarsest mesh (120 elements) to deliberately show the errors of the BEM. Even though the results on the surface for this coarse mesh contain a relatively larger error (4.93% for radial stress, Fig. 4), the results inside the domain (away from the surface) are quite good. This is one of the advantages of the BEM approach, which uses integral representation [e.g., Eq. (5)] for this calculation that tends to reduce the errors inside the domain. Note that both the radial and tangential stresses tend to the applied far-field stress σ^∞, as the distance r from the center of the sphere increases. The stress contour plot for σ_x on the surface (boundary of the medium) is given in Fig. 7 for the finest mesh (shown in Fig. 3). The boundary stress field is obtained by using the traction results and averaged at each corner node using results on the surrounding elements. Note the increase of the stress value on the surface (with a stress concentration factor of 1.6154) and its location due to the presence of the rigid sphere in the elastic medium.

The excellent agreement of the BEM results with the analytical solution for this example suggests that the developed new BIE formulation and its BEM implementation are correct and effective. Fiber-reinforced composite materials will be considered next using this rigid-inclusion model and the BEM approach.

5.2 Short-Fiber-Reinforced Composites. Modeling of fiber-reinforced composites using the rigid-inclusion model and the developed BEM is considered in this and next examples. Short fibers in a matrix are more likely to act like rigid rods [18] if their stiffness is more than an order of magnitude higher than that of the matrix. Several representative volume elements containing different numbers of fibers are used to study the interactions of the fibers and to estimate the effective properties of the composites. We limit our attention to short and moderately long fibers in a matrix, where the aspect ratio (length/diameter) of an inclusion is kept below 20. The main purpose of these examples is to show the capabilities and promises of the developed fast BEM in large-scale modeling of fiber-reinforced composites. The models studied here are simple and ideal in nature, with more realistic ones being left for future applications.

The RVEs considered in this study are of finite sizes and *embedded* in an infinite domain with the same material as that of the matrix (cf., similar inclusion models in 2D infinite space reported in Refs. [9–14,16,17]). In this way, the problem can be posed as

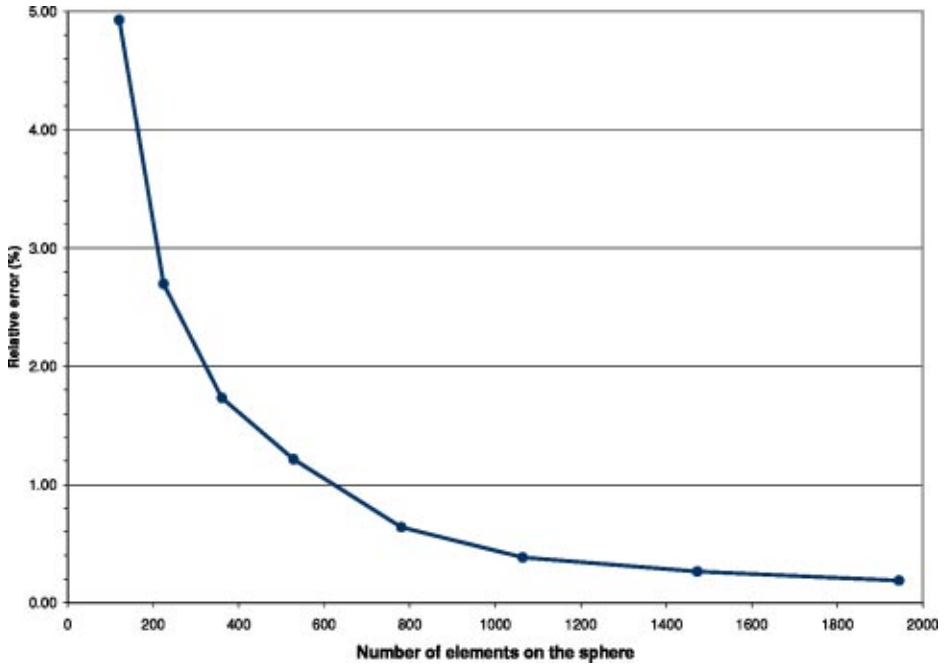

Fig. 4 Convergence of the BEM results for surface radial stress $\sigma_r(a)$

an infinite domain problem and the structure of Eq. (20) can be preserved. [A RVE model as a finite domain problem can be easily implemented with some modifications of Eq. (20) to consider direct loading on the surfaces of a RVE.] In the current embedded RVE models, a far-field uniaxial tensile stress is applied in the x-direction (Fig. 8). To estimate the effective Young's modulus of a composite in one direction (e.g., the fiber or x-direction), the displacements and stresses at some surfaces of the RVE, to be called data-collection surfaces (Fig. 8), are computed using Eq. (5) and its gradients, after the traction $\mathbf{t}$ is determined for each rigid inclusion by solving the BIE equations. The effective Young's modulus of the composite is estimated using the displacement and stress results at these data-collection surfaces by the following formula (which ignores the stresses on the lateral surfaces that have been found much smaller in value compared with σ_x in the cases studied):

$$E_{\text{eff}} = \frac{(\sigma_x)_{(\text{ave})} L}{(\Delta u_x)_{(\text{ave})}}, \tag{26}$$

where E_{eff} is the estimated effective Young's modulus of the composite in the x-direction (Fig. 8), and the displacement and stress averaged over the data-collection surfaces (Fig. 8) are obtained by:

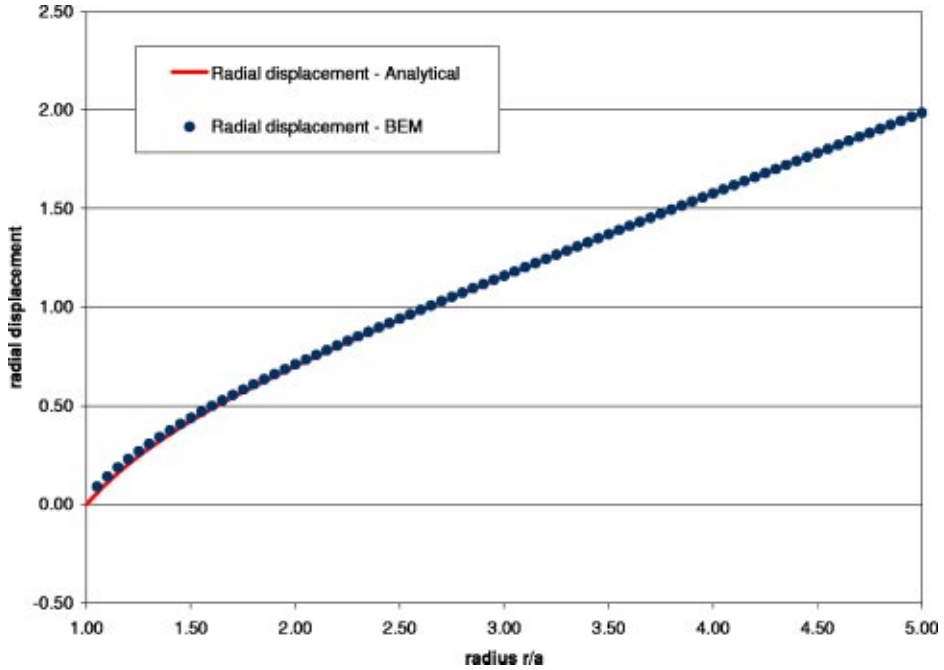

Fig. 5 Radial displacement ($\times \sigma^{\infty} a/E$) obtained by the BEM model with 120 elements

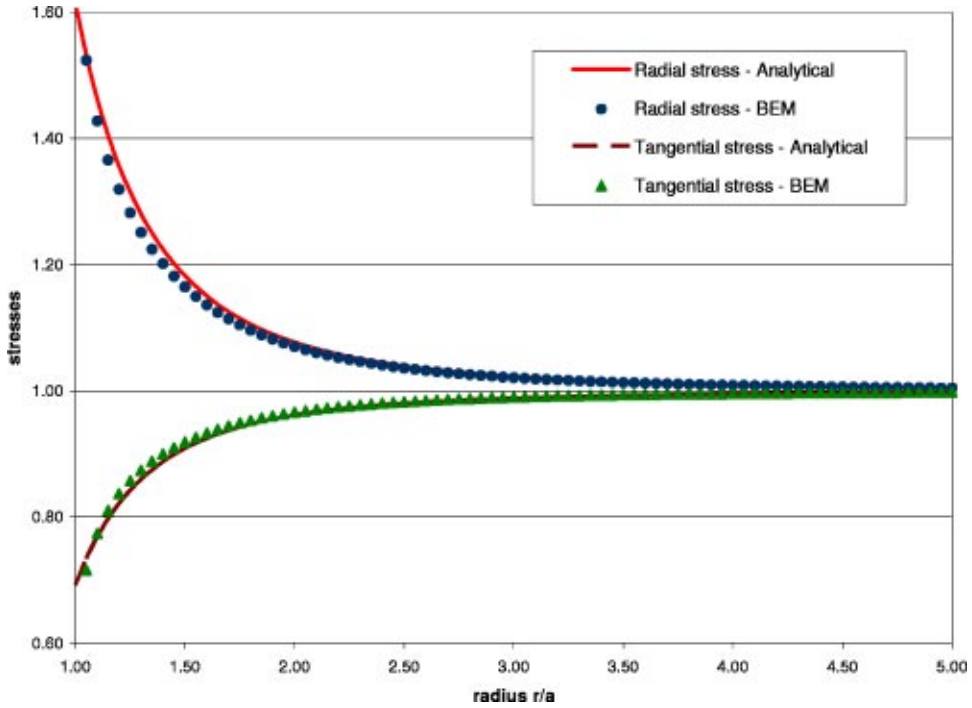

Fig. 6 Radial and tangential stresses ($\times\sigma^{\infty}$) obtained by the BEM model with 120 elements

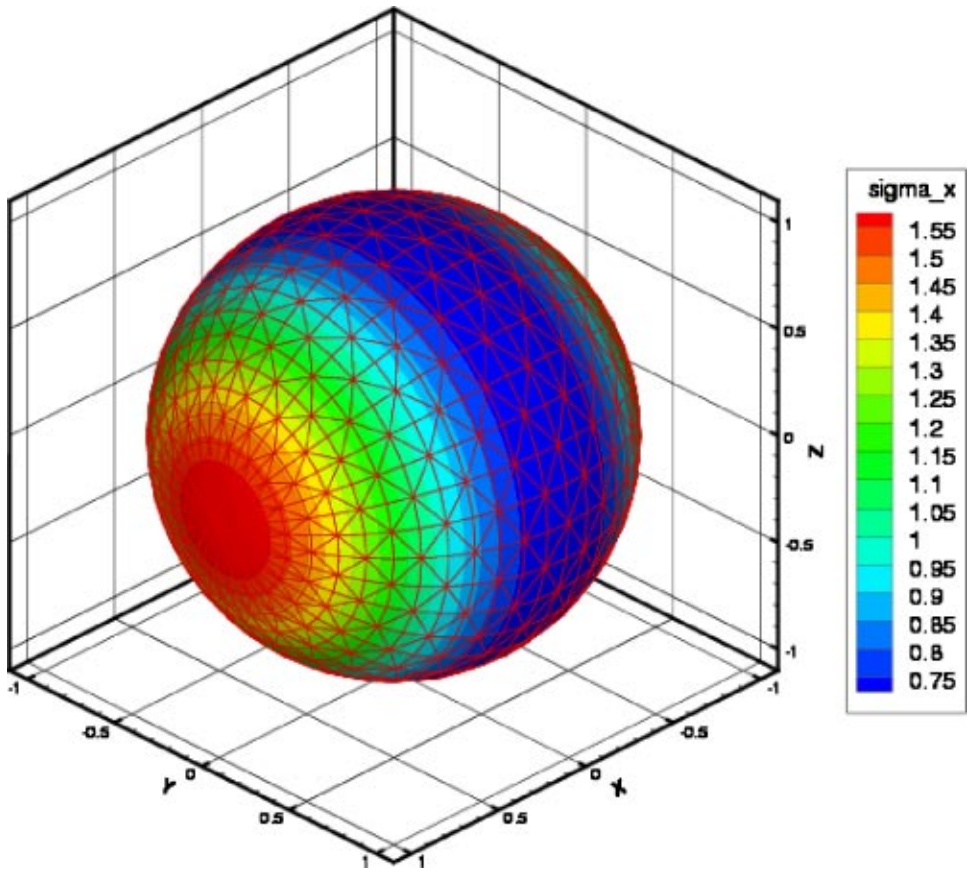

Fig. 7 Contour plot for stress $\sigma_x(\times\sigma^{\infty})$ on the surface of the rigid sphere

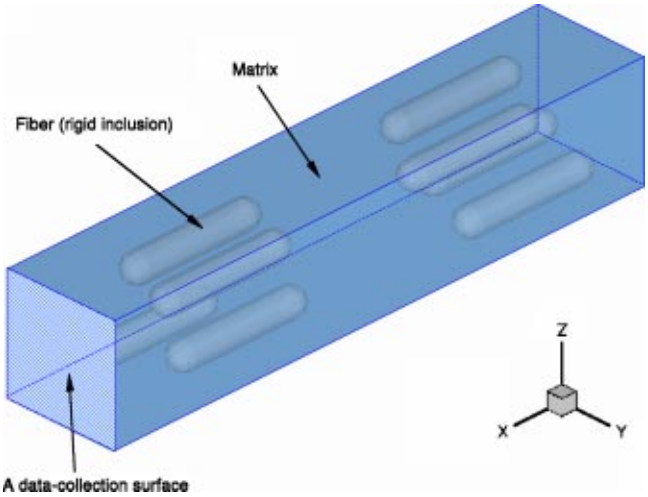

Fig. 8 A RVE of a short fiber-reinforced composite

$$(\Delta u_x)_{(\text{ave})} = (u_x(x = L/2))_{(\text{ave})} - (u_x(x = -L/2))_{(\text{ave})}, \quad (27)$$

$$(\sigma_x)_{(\text{ave})} = [(\sigma_x(x = L/2))_{(\text{ave})} + (\sigma_x(x = -L/2))_{(\text{ave})}]/2, \quad (28)$$

with L being the length of the RVE in the x direction Fig. 8, the origin of the coordinate system is located at the center of the RVE). In this way, the effective modulus is obtained as the local elastic constant of the volume with inclusions. One may argue that the effective modulus in (26) is an apparent property because it is obtained using an infinite domain that acts as part of the ''loading device.'' Indeed, the effectiveness of this approach with a RVE embedded in the infinite domain needs to be verified with other results and improved RVE models can also be developed. The reader is referred to Sec. 6 for further discussions and an attempt to verify the proposed approach.

A mesh with 456 boundary elements for a short, cylindrical fiber of an aspect ratio equal to 5 (length=50 and diameter=10) is shown in Fig. 9. This mesh is sufficient for obtaining converged results for the estimated effective moduli. The fiber is initially placed at the center of a box of dimensions $100\times20\times20$ (chosen arbitrarily) and filled with the matrix material. This box is then repeated in the x-, y-, and z-directions to generate the multiple-fiber RVE models. Three different distributions and orientations of the fibers are considered. The first case is the uniform distribution of aligned fibers, to be called the *uniform* case. The second case is a ''random'' distribution of aligned fibers, where the fibers are still aligned in the x-direction, but their locations are shifted randomly in the x-, y-, and z-directions to such an extent that each fiber remains in its own box (territory) to avoid contact of the fibers. This case is called the *aligned random* case. The third case is a ''random'' distribution and ''random'' orientation of the fibers. Again the random distribution and (small angle) rotation of a fiber is limited to the extent that it remains in its own box. This case is named the *random* (or to be more precise, a *controlled* random) case. In all the cases, the volume fraction of the fiber is 9.16% based on the dimensions of the RVE and fibers. A Poisson's ratio of 0.3 is used for the matrix.

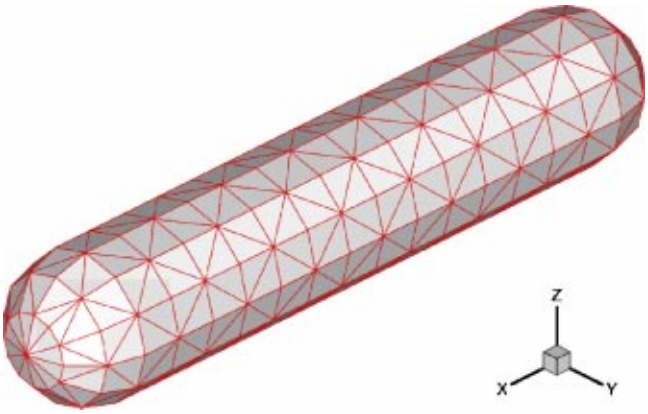

Fig. 9 A BEM mesh used for the short fiber inclusion (with 456 elements)

Figure 10 shows the contour plot of surface stress σ_x (in the matrix) for the RVE containing 216 ''random'' short fibers. For each fiber, high stresses occur around the two ends of the fiber, which is consistent with the theory that in the limit as the slender inclusion becomes a rigid line, singularity of stresses will arise at the two tips [9]. Values of these stresses are even higher when two fibers are closer to each other, suggesting closer interactions of the fibers. This stress plot is typical among all the studied RVEs containing $q\times q\times q$ fibers, with $q=2$, 3, 4, 6, 8, 10, 12, and 13 in this example. The largest RVE with 2197 (an array of $13\times13\times13$) ''random'' fibers is shown in Fig. 11. The total degrees of freedom for the model in Fig. 11 is 3 018 678 ($=2197\times(6+456\times3)$).

The normalized Young's moduli ($E_{\text{eff}}/E_{\text{matrix}}$) of the composites, estimated with the three different fiber distributions and orientations using the above mentioned RVEs, are plotted in Fig. 12. The increase of the effective Young's modulus of the composite estimated by the RVEs with uniform distributions of aligned fibers ranges from 28.1% to 40.8% (a difference of 45.2%) as the number of fibers (or size of the RVEs) increases from 8 to 2197. The values of the modulus in this uniform case increase gradually and tend to a constant value. These results suggest that a RVE with a smaller number of short fibers is inefficient for obtaining the effective properties accurately with Eq. (26) even in the cases with uniform distributions of aligned fibers (without considering the periodic boundary conditions). The estimated increases of the Young's moduli in the *aligned random* and *random* cases range from 27.7% to 46.2% and oscillate within this range until approaching another constant. Surprisingly, the estimated moduli in the aligned random and random cases are higher for most RVEs than those in the corresponding uniform case. This may suggest that the load transfer may be improved by the ''random'' distributions of fibers in a short-fiber composite. However, in comparison, the values of the effective moduli are about 30% lower than those predicted by the theory and BEM (for incompressible materials) reported in Ref. [18] for the same fiber volume fraction and aspect ratio. This may be due to the fact that the fibers in the current models are confined within their own boxes and no ''relays'' occur in the fiber direction, even in the ''random'' case, which leads to ''weakest-link'' regions between two arrays of fibers. While in the models used in Ref. [18], aligned fibers are placed randomly in the RVE and therefore better load transfer are achieved. Further tests on the current BEM can be carried out with more realistic distributions of the fibers.

Figure 13 shows the CPU time used to obtain results in this short-fiber composite example, on a FUJITSU PRIMEPOWER HPC2500 machine (a shared memory machine with 96 CPUs and 384GB memory) and using four CPUs. In this example, no serious attempts have been made to parallelize the code except for the automatic parallelization made by the compiler. Contrary to the traditional BEM where the solution time is of $O(N^3)$ (with N here being the total number of DOFs), the CPU time required for solving a model using the fast multipole BEM is only of $O(N)$ as shown in Fig. 13 (a straight line with the slope close to unity). Furthermore, the memory required for solving a problem also increases linearly with the size of the problem for fast multipole BEM. Also, the number of iterations required to reach the convergence with a tolerance of 10^{-5} in using the GMRES is between 5 (for $N=10\,992$) and 7 (for $N=3\,018\,678$). Therefore, the fast

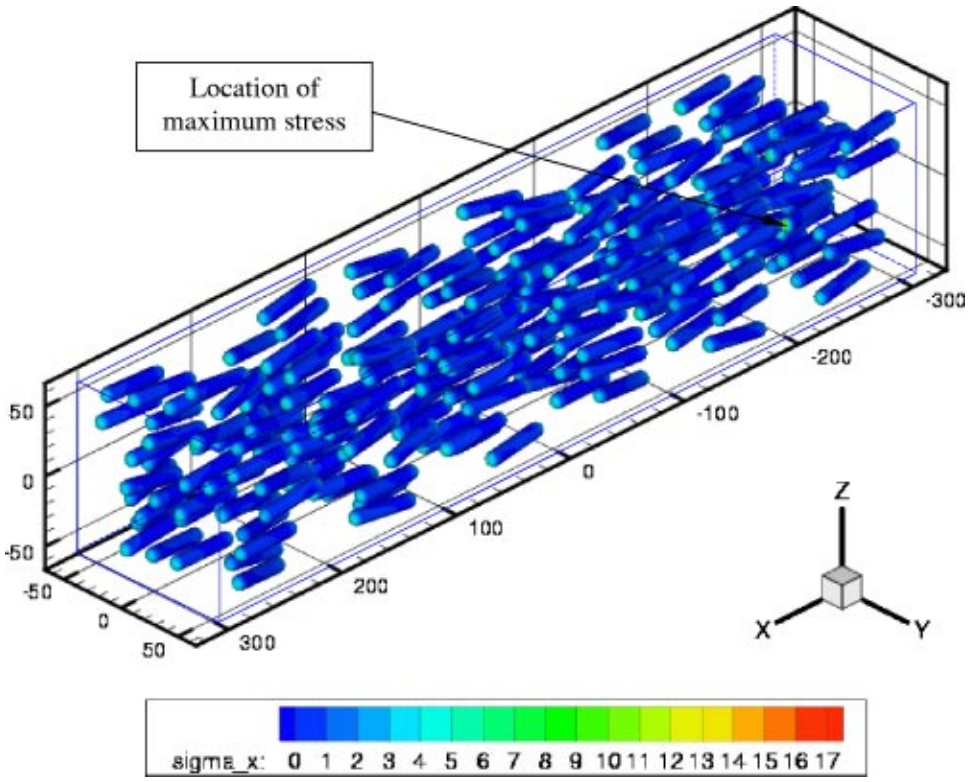

Fig. 10 Contour plot of surface stresses ($\times\sigma^{\infty}$) for a model with 216 "randomly" distributed and oriented short fibers

multipole BEM is much faster and more efficient as compared with the traditional BEM (further discussions and examples can be found in Refs. [21,39]).

These preliminary results in modeling short-fiber-reinforced composites clearly demonstrate the effectiveness and robustness of the developed fast multipole BEM based on the rigid-inclusion model.

5.3 Long-Fiber-Reinforced Composites. Composites reinforced with relatively long fibers, with an aspect ratio of 16 (length=80 and diameter=5), are studied using the developed BEM. Each fiber is discretized using 600 boundary elements and placed in a box of the same dimensions ($100\times20\times20$) as in the short-fiber example. This box is then repeated in the *x*-, *y*-, and *z*-directions to generate RVEs containing $q\times q\times q$ fibers, with q

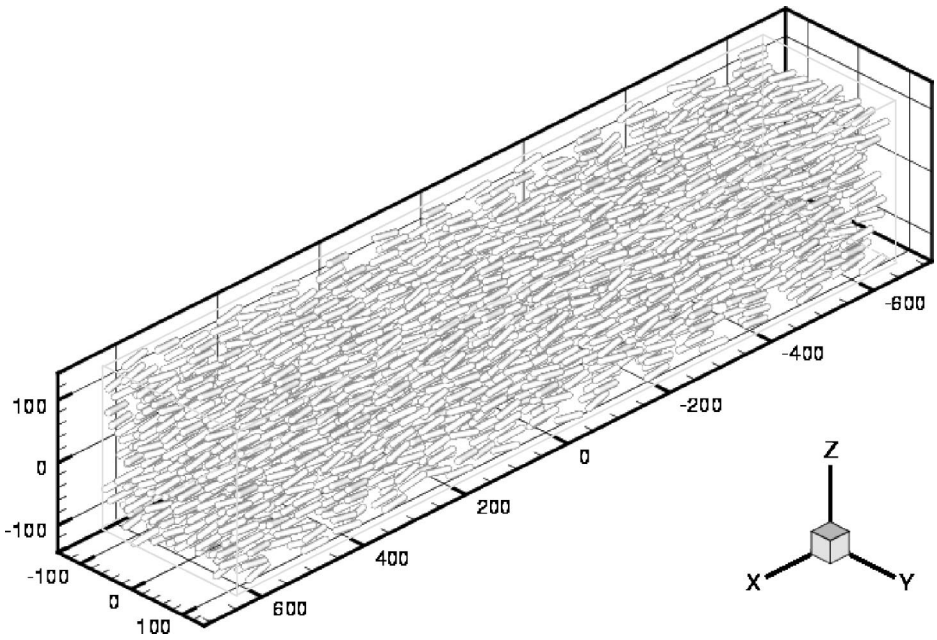

Fig. 11 A RVE containing 2197 short fibers with the total DOF=3 018 678

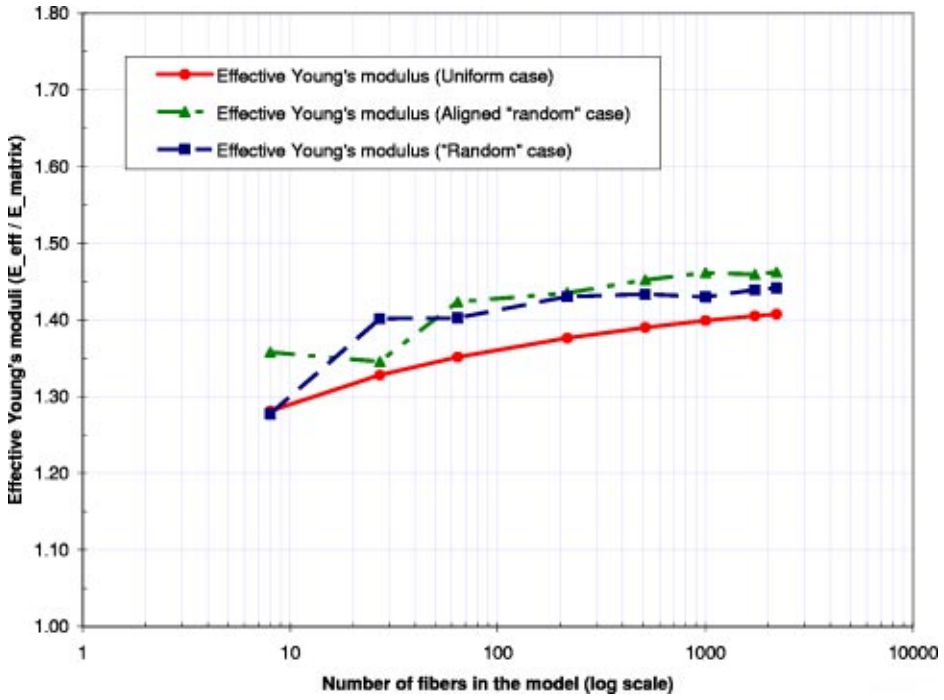

Fig. 12 Estimated effective Young's moduli in the *x*-direction for the composite model with up to 2197 *short* rigid fibers (fiber volume fraction=9.16%)

=2, 3, 4, 6, 8, 10, 12, 13, 15, and 18 in this example. The largest model with 5832 fibers and 10 532 592 DOFs (5832×(6+600 ×3)) is shown in Fig. 14. The fibers are arranged in the so called ''random'' manner as in the short-fiber RVEs. Again, these are ''controlled random'' distributions (each fiber within its own box) and orientations (with small rotation angles) of the fibers so that no contact among them occur in the RVEs. The volume fraction of the fiber is 3.85% for all the long-fiber models in this example. The Poisson's ratio for the matrix is 0.3.

Figure 15 shows the normalized effective Young's moduli ($E_{\text{eff}}/E_{\text{matrix}}$) computed for the composites with the relatively long fibers using the RVEs in the uniform and ''random'' cases. The increases of the computed effective moduli are about two times higher in these long-fiber cases than those in the short-fiber cases, even though the fiber volume fraction is lower. This is expected since aligned long fibers are better for load transfer in a composite. The increases in the values of the modulus range from 75.9% to 95.0% for the uniform case and from 65.4% to 87.6% for the

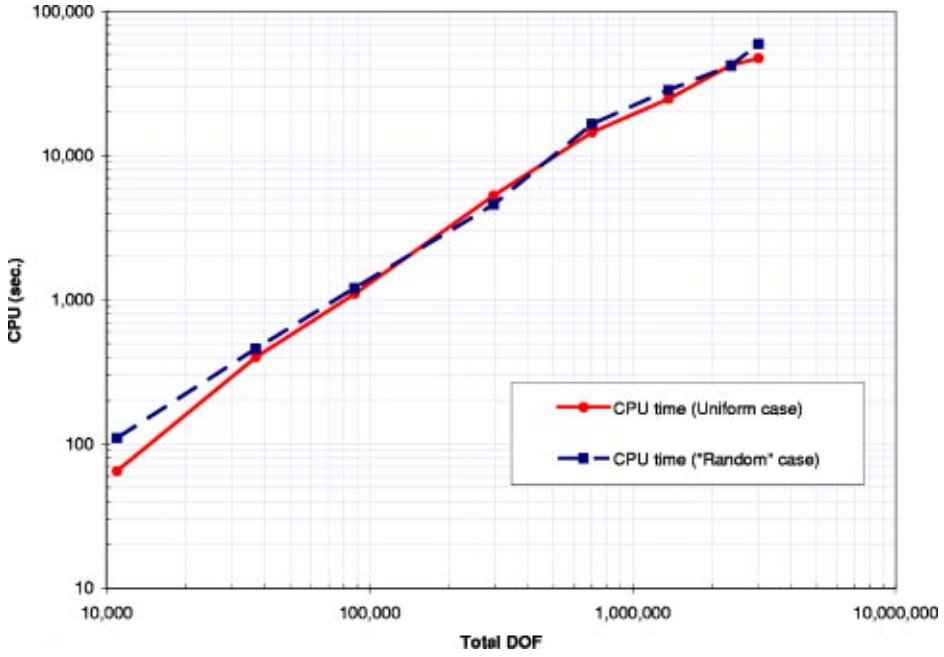

Fig. 13 CPU time used for solving the BEM models for the short-fiber cases

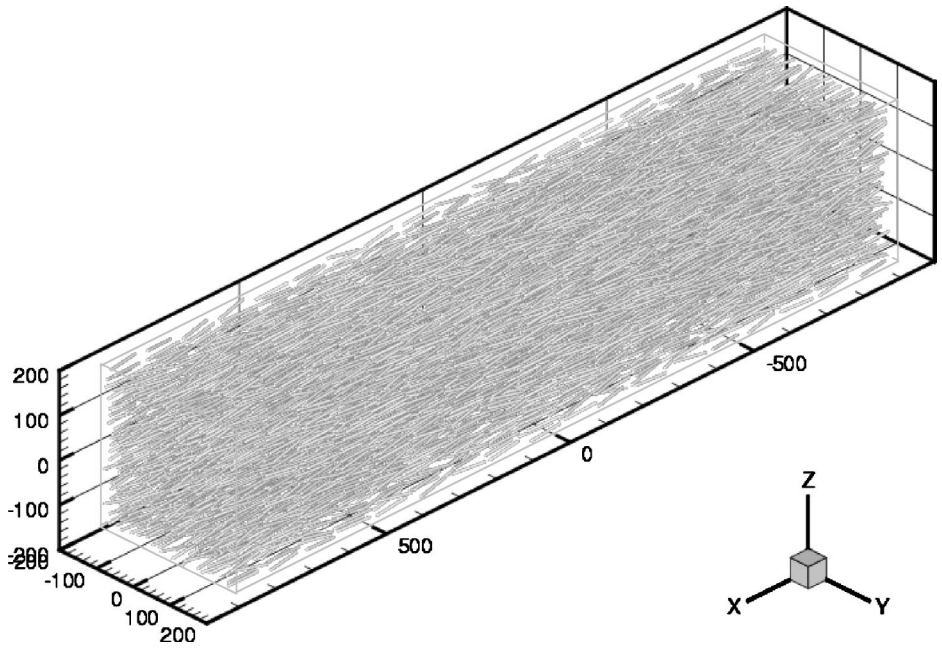

Fig. 14 A RVE containing 5832 long fibers with the total DOF=10 532 592

random case. Results for the uniform case increase gradually with the increase of the RVE sizes and tend to a constant value (95.0%). The values obtained for the ''random'' case fluctuate for the smaller RVEs and also approach a constant for the larger RVEs. However, the increases in the ''random'' case are about 8% lower than those in the uniform case in this long-fiber example. This suggests that even small misalignment and rotations of long fibers (which are uniformly and closely packed in the fiber direction initially) will offset the enhancement in the stiffness for long-fiber composites. The largest RVE model (with 5832 fibers and 10 532 592 DOFs) can be solved in 3 h and 40 min (wall-clock time) on the PRIMEPOWER HPC2500 computer using 32 CPUs, with a tolerance of 10^{-5} in the solution with GMRES and ten-term expansion in the FMM. The code used for this example was parallelized with minimum efforts using OpenMP and automatic parallelization option of the compiler.

Rapid convergence is achieved in this case also. The number of iterations in solving the preconditioned system using the GMRES iterative solver is between 5 (for $N=14\,448$) and 11 (for $N=10\,532\,592$) with a tolerance of 10^{-5}. This shows that the preconditioner in (22) works very well even in problems when the

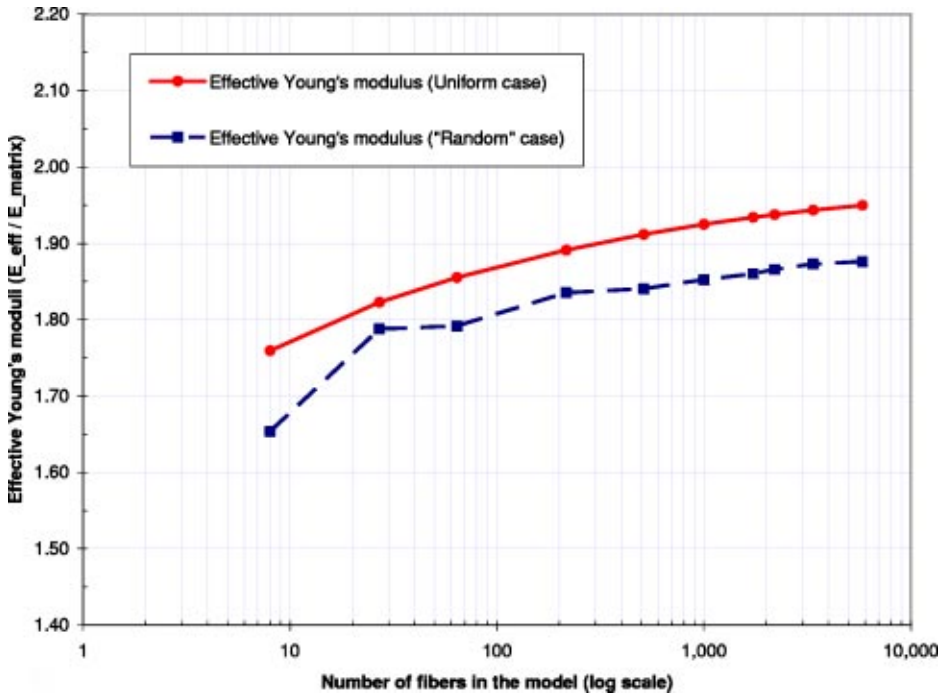

Fig. 15 Estimated effective Young's moduli in the *x*-direction for the composite model with up to 5832 *long* rigid fibers (fiber volume fraction=3.85%)

aspect ratio of the inclusions is as large as 16. The robustness of the developed BEM for modeling fiber-reinforced composites is demonstrated again by this example which has reached 10 million DOFs for the boundary element method.

6 Discussions

The developed fast multipole BEM for the analysis of fiber-reinforced composites based on the rigid-inclusion model has been demonstrated to be very effective and efficient for large scale models. Interactions of the fibers, load transfer mechanisms and effective properties of a composite can be investigated readily using the BEM code with different parameters, such as fiber aspect ratios, volume fractions, waviness, distributions, and orientations. However, further studies are needed regarding the effectiveness of the model and method for evaluating the effective properties of the composite materials, since the rigid-inclusion model has some obvious limitations. For example, the effect of the ratio of the Young's modulus of the fiber to that of the matrix for a composite can not be accounted for in the rigid-inclusion model (this ratio is equal to infinity in the rigid model for any matrix material). Although there are a large amount of experimental data and numerous analytical results based on different theories for estimating the effective properties of fiber-reinforced composites, direct comparison of the BEM results with these data was not attempted in this study (except with that in Ref. [18]), because of the wide variations in those data. More realistic models of the fiber-reinforced composites using the rigid or elastic inclusion approaches need to be studied using the developed BEM in future applications.

The boundary integral equation developed for this study, Eq. (6), is essentially an integral equation of the first kind, which, used in its original form, may raise the question of stability and convergence of its solutions when using iterative solvers as in the FMM. Our experience has shown that even for integral equations of the first kind, the FMM BEM, which uses iterative solvers such as GMRES, can still deliver fast converging and stable results with good preconditioners. Our selection of using the right preconditioner in Eq. (22) turns out to be very effective.

The RVE used in this study is of finite size as shown in Fig. 8, that is embedded in an infinite space filled with the matrix material and loaded remotely (cf., again, 2D models in infinite space used in Refs. [9–14,16,17]). This is chosen so that an infinite domain problem can be solved, which is easier to handle concerning the boundary conditions and, in general, converges faster than an interior problem using the FMM. In this infinite domain problem, the displacement and stress fields on the surfaces of the RVE (data-collection surfaces) need to be calculated after the boundary solutions on all the inclusions are obtained with the fast multipole BEM. This calculation of the fields inside the domain takes extra CPU time, which can be substantial for large models, although it can be computed by using the FMM also [30]. An interior problem defined on the finite sized RVE directly can certainly be implemented with some modifications of Eq. (20) and may provide some improvements to the current RVE model. For example, the boundary solutions (displacements and tractions) on the RVE surfaces, which are available after the solution of an interior problem, can be used directly to evaluate the effective properties. A more reliable, and perhaps more elegant, approach for computing the effective modulus is to use FMM for periodic boundary conditions [25]. Our preliminary analysis with the two dimensional Laplace problems [17] shows that the periodic FMM BEM can be implemented easily, and the increase of the CPU time over the ordinary FMM is less than 20%. The effective property obtained with an equivalent formula of (26) and with the periodic FMM did not differ very much. The elastic counterpart of the periodic FMM is now underway.

The rigid-inclusion model for fiber-reinforced composites may have the potential in some very urgent applications, such as modeling of the emerging carbon nanotube (CNT)-based composites (see, e.g., Refs. [42–45]). The Young's moduli of carbon nanotubes are in general greater than 1 TPa along the tube direction, about two orders higher than those of many matrix materials [43,44]. To model the CNT-based composites, continuum mechanics approaches using the FEM or BEM [46–49] may still be applied if the overall behaviors and properties of the CNT-based composites are to be investigated. However, CNTs are usually produced in different shapes and sizes (for example, being curved, twisted, or bundled), and are difficult to align in a composite. Thus the computational models for such composites may need to contain a much larger number of fibers in a RVE, as compared to those for traditional composites for which the fibers can be aligned easily and distributed uniformly, mainly because of their larger scales. The BEM can model multimaterial problems easily since it uses elements only on boundaries and interfaces of the problem domain. With the fast multipole BEM, the solution time has also been reduced dramatically for large-scale problems. The rigid-inclusion model further simplifies the BEM approach and increases its efficiency in the analysis of some special composite materials, as demonstrated by the examples in the previous section. All these features and new development make the BEM very appealing in large scale analysis of CNT-based composites for estimating their overall mechanical properties. Studies are underway along this line in modeling CNT-based composites by using the developed fast multipole BEM with new interface conditions based on molecular dynamics simulations of CNT-fiber pullout tests.

The work reported in this paper, on using the rigid-inclusion models for analyzing fiber-reinforced composites, is only the first step in the development of a more general FMM BEM for studying such materials and many others. The developed BIE formulation and the FMM BEM can be extended readily for other problems. A FMM BEM solver for general inclusion problems can be developed, where the inclusions can be elastic or rigid, or simply a void. Other RVE models, for example, with periodic boundary conditions, can be implemented as stated above. Interfacing the developed BEM with other methods (such as molecular dynamics) for multiscale analyses of CNT-based composites can also be considered and may present unique advantages over other domain-based methods. Higher-order boundary elements can be applied to further increase the efficiency and accuracy of the BEM. A practical and important development for the BEM code is to develop an improved preprocessor that can generate the boundary element mesh for a RVE containing a large number of truly randomly distributed and oriented fibers, including curved ones, so that more realistic models of composites can be analyzed based on real experimental or fabrication parameters. Finally, full parallelization of the BEM code can be implemented to further increase the robustness of the developed fast multipole BEM for even larger models based, eventually, directly on scanned 3D models of composite material samples.

7 Conclusion

A new boundary integral equation formulation for the analysis of an elastic medium containing rigid inclusions is derived in this paper. This new BIE contains only the weakly-singular displacement kernel from the fundamental solution and thus is much more efficient to solve than the traditional singular BIE. The fast multipole boundary element method is employed to solve this new BIE. The developed BIE formulation and FMM BEM code are found to be very stable and the results converge in about 10 iterations for a tolerance of 10^{-5} with the preconditioned GMRES. The numerical results for a spherical rigid inclusion in an elastic domain match very closely with the analytical solution. Short- and moderately long-fiber-reinforced composites are investigated using the developed BEM and their effective Young's moduli are estimated using the BEM displacement and stress results for the representative volume elements. The largest model studied contains more than 5800 fibers and has the total degrees of freedom

over 10 millions. These preliminary results clearly demonstrate the effectiveness, efficiency and promises of the developed fast multipole BEM for studying fiber-reinforced composites, when the fibers are much stiffer than the matrix material.

Acknowledgments

Y.J.L. would like to acknowledge the support by the Academic Center for Computing and Media Studies of the Kyoto University and the fellowship of the Japan Society for the Promotion of Science (JSPS). The authors thank the three reviewers for their valuable comments about this paper.

References

[1] Mackerle, J., 1994, ''Finite Element and Boundary Element Library for Composites—A Bibliography (1991–1993),'' Finite Elem. Anal. Design, **17**, pp. 155–165.
[2] Achenbach, J. D., and Zhu, H., 1989, ''Effect of Interfacial Zone on Mechanical Behavior and Failure of Fiber-Reinforced Composites,'' J. Mech. Phys. Solids, **37**, pp. 381–393.
[3] Zhu, H., and Achenbach, J. D., 1991, ''Effect of Fiber-Matrix Interphase Defects on Microlevel Stress States at Neighboring Fibers,'' J. Compos. Mater., **25**, pp. 224–238.
[4] Gulrajani, S. N., and Mukherjee, S., 1993, ''Sensitivities and Optimal Design of Hexagonal Array Fiber Composites With Respect to Interphase Properties,'' Int. J. Solids Struct., **30**, pp. 2009–2026.
[5] Pan, L., Adams, D. O., and Rizzo, F. J., 1998, ''Boundary Element Analysis for Composite Materials and a Library of Green's Functions,'' Comput. Struct., **66**, pp. 685–693.
[6] Liu, Y. J., Xu, N., and Luo, J. F., 2000, ''Modeling of Interphases in Fiber-Reinforced Composites Under Transverse Loading Using the Boundary Element Method,'' J. Appl. Mech., **67**, pp. 41–49.
[7] Liu, Y. J., and Xu, N., 2000, ''Modeling of Interface Cracks in Fiber-Reinforced Composites With the Presence of Interphases Using the Boundary Element Method,'' Mech. Mater., **32**, pp. 769–783.
[8] Chen, X. L., and Liu, Y. J., 2001, ''Multiple-Cell Modeling of Fiber-Reinforced Composites With the Presence of Interphases Using the Boundary Element Method,'' Comput. Mater. Sci., **21**, pp. 86–94.
[9] Dundurs, J., and Markenscoff, X., 1989, ''A Green's Function Formulation of Anticracks and Their Interaction With Load-Induced Singularities,'' J. Appl. Mech., **56**, pp. 550–555.
[10] Hu, K. X., and Chandra, A., 1993, ''Interactions Among General Systems of Cracks and Anticracks—An Integral-Equation Approach,'' J. Appl. Mech., **60**, pp. 920–928.
[11] Hu, K. X., and Huang, Y., 1993, ''A Microcracked Solid Reinforced by Rigid-Line Fibers,'' Compos. Sci. Technol., **49**, pp. 145–151.
[12] Hu, K. X., Chandra, A., and Huang, Y., 1994, ''On Crack, Rigid-Line Fiber, and Interface Interactions,'' Mech. Mater., **19**, pp. 15–28.
[13] Chandra, A., Huang, Y., Wei, X., and Hu, K. X., 1995, ''A Hybrid Micro-Macro BEM Formulation for Micro-Crack Clusters in Elastic Components,'' Int. J. Numer. Methods Eng., **38**, pp. 1215–1236.
[14] Huang, Y., Hu, K. X., and Chandra, A., 1995, ''Stiffness Evaluation for Solids Containing Dilute Distributions of Inclusions and Microcracks,'' J. Appl. Mech., **62**, pp. 71–77.
[15] Leite, L. G. S., Coda, H. B., and Venturini, W. S., 2003, ''Two-Dimensional Solids Reinforced by Thin Bars Using the Boundary Element Method,'' Eng. Anal. Boundary Elem., **27**, pp. 193–201.
[16] Dong, C. Y., Lo, S. H., and Cheung, Y. K., 2003, ''Interaction Between Cracks and Rigid-Line Inclusions by an Integral Equation Approach,'' Comput. Mech., **31**, pp. 238–252.
[17] Nishimura, N., and Liu, Y. J., 2004, ''Thermal Analysis of Carbon-Nanotube Composites Using a Rigid-Line Inclusion Model by the Boundary Integral Equation Method,'' Comput. Mech., (in press).
[18] Ingber, M. S., and Papathanasiou, T. D., 1997, ''A Parallel-Supercomputing Investigation of the Stiffness of Aligned, Short-Fiber-Reinforced Composites Using the Boundary Element Method,'' Int. J. Numer. Methods Eng., **40**, pp. 3477–3491.
[19] Primo, A. R. M., Wrobel, L. C., and Power, H., 2000, ''Boundary Integral Formulation for Slow Viscous Flow in a Deforming Region Containing a Solid Inclusion,'' Eng. Anal. Boundary Elem., **24**, pp. 53–63.
[20] Kit, H. S., Mykhas'skiv, V. V., and Khaj, O. M., 2002, ''Analysis of the Steady Oscillations of a Plane Absolutely Rigid Inclusion in a Three-Dimensional Elastic Body by the Boundary Element Method,'' J. Appl. Math. Mech., **66**, pp. 817–824.
[21] Nishimura, N., 2002, ''Fast Multipole Accelerated Boundary Integral Equation Methods,'' Appl. Mech. Rev., **55**, pp. 299–324.
[22] Greengard, L., and Helsing, J., 1998, ''On the Numerical Evaluation of Elastostatic Fields in Locally Isotropic Two-Dimensional Composites,'' J. Mech. Phys. Solids, **46**, pp. 1441–1462.
[23] Greengard, L., Kropinski, M. C., and Mayo, A., 1996, ''Integral Equation Methods for Stokes Flow and Isotropic Elasticity in the Plane,'' J. Comput. Phys., **125**, pp. 403–414.
[24] Helsing, J., 1995, ''An Integral Equation Method for Elastostatics of Periodic Composites,'' J. Mech. Phys. Solids, **43**, pp. 815–828.
[25] Greengard, L., and Rokhlin, V., 1987, ''A Fast Algorithm for Particle Simulations,'' J. Comput. Phys., **73**, pp. 325–348.
[26] Fu, Y., Klimkowski, K. J., Rodin, G. J., Berger, E., Browne, J. C., Singer, J. K., Geijn, R. A. V. D., and Vemaganti, K. S., 1998, ''A Fast Solution Method for Three-Dimensional Many-Particle Problems of Linear Elasticity,'' Int. J. Numer. Methods Eng., **42**, pp. 1215–1229.
[27] Peirce, A. P., and Napier, J. A. L., 1995, ''A Spectral Multipole Method for Efficient Solution of Large-Scale Boundary Element Models in Elastostatics,'' Int. J. Numer. Methods Eng., **38**, pp. 4009–4034.
[28] Popov, V., and Power, H., 2001, ''An $O(N)$ Taylor Series Multipole Boundary Element Method for Three-Dimensional Elasticity Problems,'' Eng. Anal. Boundary Elem., **25**, pp. 7–18.
[29] Nishimura, N., Yoshida, K., and Kobayashi, S., 1999, ''A Fast Multipole Boundary Integral Equation Method for Crack Problems in 3D,'' Eng. Anal. Boundary Elem., **23**, pp. 97–105.
[30] Yoshida, K., Nishimura, N., and Kobayashi, S., 2001, ''Application of Fast Multipole Galerkin Boundary Integral Equation Method to Crack Problems in 3D,'' Int. J. Numer. Methods Eng., **50**, pp. 525–547.
[31] Lai, Y.-S., and Rodin, G. J., 2003, ''Fast Boundary Element Method for Three-Dimensional Solids Containing Many Cracks,'' Eng. Anal. Boundary Elem., **27**, pp. 845–852.
[32] Rizzo, F. J., 1967, ''An Integral Equation Approach to Boundary Value Problems of Classical Elastostatics,'' Q. Appl. Math., **25**, pp. 83–95.
[33] Rizzo, F. J., Shippy, D. J., and Rezayat, M., 1985, ''A Boundary Integral Equation Method for Radiation and Scattering of Elastic Waves in Three Dimensions,'' Int. J. Numer. Methods Eng., **21**, pp. 115–129.
[34] Mukherjee, S., 1982, *Boundary Element Methods in Creep and Fracture*, Applied Science Publishers, NY.
[35] Banerjee, P. K., 1994, *The Boundary Element Methods in Engineering*, 2nd ed., McGraw–Hill, NY.
[36] Brebbia, C. A., and Dominguez, J., 1989, *Boundary Elements—An Introductory Course*, McGraw–Hill, NY.
[37] Kane, J. H., 1994, *Boundary Element Analysis in Engineering Continuum Mechanics*, Prentice–Hall, Englewood Cliffs, NJ.
[38] Takahashi, T., Kobayashi, S., and Nishimura, N., 1999, ''Fast Multipole BEM Simulation of Overcoring in an Improved Conical-End Borehole Strain Measurement Method,'' in *Mechanics and Engineering—In Honor of Professor Qinghua Du's 80th Anniversary*, edited by Yao, Z. H., Tsinghua University Press, Beijing, pp. 120–127.
[39] Yoshida, K., 2001, ''Applications of Fast Multipole Method to Boundary Integral Equation Method,'' Ph.D. dissertation, Department of Global Environment Engineering, Kyoto University.
[40] Timoshenko, S. P., and Goodier, J. N., 1987, *Theory of Elasticity*, 3rd ed., McGraw–Hill, NY.
[41] Mura, T., 1987, *Micromechanics of Defects in Solids*, 2nd revised ed., Kluwer Academic, Dordrecht.
[42] Thostenson, E. T., Ren, Z. F., and Chou, T.-W., 2001, ''Advances in the Science and Technology of Carbon Nanotubes and Their Composites: A Review,'' Compos. Sci. Technol., **61**, pp. 1899–1912.
[43] Ruoff, R. S., and Lorents, D. C., 1995, ''Mechanical and Thermal Properties of Carbon Nanotubes,'' Carbon, **33**, pp. 925–930.
[44] Lu, J. P., 1997, ''Elastic Properties of Single and Multilayered Nanotubes,'' J. Phys. Chem. Solids, **58**, pp. 1649–1652.
[45] Qian, D., Dickey, E. C., Andrews, R., and Rantell, T., 2000, ''Load Transfer and Deformation Mechanisms in Carbon Nanotube-Polystyrene Composites,'' Appl. Phys. Lett., **76**, pp. 2868–2870.
[46] Fisher, F. T., Bradshaw, R. D., and Brinson, L. C., 2002, ''Effects of Nanotube Waviness on the Modulus of Nanotube-Reinforced Polymers,'' Appl. Phys. Lett., **80**, pp. 4647–4649.
[47] Fisher, F. T., Bradshaw, R. D., and Brinson, L. C., 2003, ''Fiber Waviness in Nanotube-Reinforced Polymer Composites—I: Modulus Predictions Using Effective Nanotube Properties,'' Compos. Sci. Technol., **63**, pp. 1689–1703.
[48] Liu, Y. J., and Chen, X. L., 2003, ''Evaluations of the Effective Materials Properties of Carbon Nanotube-Based Composites Using a Nanoscale Representative Volume Element,'' Mech. Mater., **35**, pp. 69–81.
[49] Chen, X. L., and Liu, Y. J., 2004, ''Square Representative Volume Elements for Evaluating the Effective Material Properties of Carbon Nanotube-Based Composites,'' Comput. Mater. Sci., **29**, pp. 1–11.